Enhancing strength and range of atom-atom interaction in a coupled-cavity array via parametric drives

Ya-long Ren,[1,2] Sheng-li Ma,[1,*] Stefano Zippilli,[2,†] David Vitali,[2,3,4] and Fu-li Li[1]

[1]*MOE Key Laboratory for Nonequilibrium Synthesis and Modulation of Condensed Matter and Shaanxi Province Key Laboratory of Quantum Information and Quantum Optoelectronic Devices, School of Physics, Xi'an Jiaotong University, Xi'an 710049, People's Republic of China*

[2]*Physics Division, School of Science and Technology, University of Camerino, I-62032 Camerino, Italy*

[3]*Istituto Nazionale di Fisica Nucleare, Sezione di Perugia, via A. Pascoli, I-06123 Perugia, Italy*

[4]*Consiglio Nazionale dell Richerce-Instituto Nazionale di Ottica, L.go Enrico Fermi 6, I-50125 Firenze, Italy*

(Received 14 May 2023; accepted 14 September 2023; published 26 September 2023)

Coherent long-range interactions between atoms are a prerequisite for numerous applications in the field of quantum information science. Here we present an appealing method to dramatically enhance the long-range atom-atom interaction mediated by a coupled-cavity array that is subjected to two-photon (parametric) drives. Our method allows one to greatly amplify both the localization length of the single-photon bound-state wave function and the effective atom-photon coupling strength, resulting in a significant improvement of photon-mediated coherent interaction between two distant atoms. Additionally, we illustrate this effect by analyzing how it facilitates the transfer of information and the creation of entanglement between the atoms.

DOI: 10.1103/PhysRevA.108.033717

I. INTRODUCTION

The pursuit of coherent interactions between atomic emitters, such as neutral atoms, solid-state spins, and superconducting qubits, is a central topic of interest in the quantum information science community [1–4]. In fact, it can activate a variety of important applications, including quantum annealing [5], quantum sensing [6], quantum cryptography [7], quantum computation [8], and quantum simulation [9]. In particular, strong long-range atom-atom interactions lie at the heart of this subject, unlocking opportunities for long-distance quantum logic gates [10,11] and entanglement generation and distribution [12,13]. Additionally, long-range couplings could trigger a series of exciting phenomena, such as dynamical quantum phase transitions [14], nonadditivity in statistical mechanics [15], exotic long-range order [16], and the violation of the Lieb-Robinson bound on the speed of information propagation [17]. To realize long-range interactions between atoms, a mainstream solution is to interface the atoms with a photonic waveguide and exploit the exchange of virtual photons [18–25]. However, in this case, the resulting photon-mediated interactions are considerably suppressed with the increase of the atomic separation.

In this work, we put forward a feasible method to substantially enhance the long-range atom-atom interaction in a coupled-cavity array. We show that, when each photonic site of the array is subjected to a two-photon drive, both the localization length of the single-photon bound-state wave function and the effective atom-photon coupling strength can be amplified greatly. Accordingly, when two distant atoms are both coupled to the photonic array in the dispersive regime, the photon-mediated atom-atom interaction is strongly enhanced in terms of both range and strength, pushing it from the weak coupling regime into the strong coupling regime. As a concrete application, we show that, even with a relatively large interatomic distance, quantum entanglement and quantum state transfer between two separated atoms can still be efficiently generated. Finally, we emphasize that our model is quite general and can be implemented with different kinds of architectures, such as superconducting qubits coupled to a microwave cavity array [20,23–27] and atomic emitters coupled to an optical cavity array [28–32].

II. THE SETUP

As schematically shown in Fig. 1(a), we consider a coupled atom-photon system, where two atoms with excited state $|e_x\rangle$ $(x = A, B)$ and ground state $|g_x\rangle$ interact with a one-dimensional coupled-cavity array. The corresponding Hamiltonian reads (setting $\hbar = 1$)

$$H_a = \omega_a \sum_n a_n^\dagger a_n + \omega_q \sum_x \sigma_+^x \sigma_-^x - \left[J \sum_n a_n^\dagger a_{n+1} - G(a_j^\dagger \sigma_-^A + a_l^\dagger \sigma_-^B) + \text{H.c.} \right], \quad (1)$$

where a_n $(a_n^\dagger)$ is the bosonic annihilation (creation) operator of the nth cavity with the index $n \in [-N, N]$, $\sigma_-^x = |g_x\rangle\langle e_x|$ $(\sigma_+^x = |e_x\rangle\langle g_x|)$ is the atomic lowering (raising) operator, and ω_a and ω_q are the resonance frequency of the cavities and atoms, respectively. J is the cavity-cavity nearest-neighbor coupling strength, and G is the atom-cavity coupling strength.

*msl1987@xjtu.edu.cn
†stefano.zippilli@unicam.it

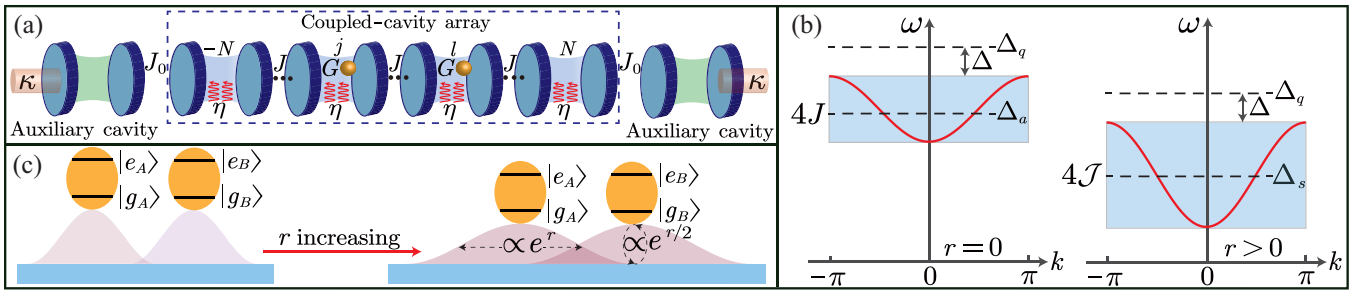

FIG. 1. (a) Schematic illustration of the setup: two distant atom are coherently coupled to a coupled-cavity array that is subjected to two-photon drives, and the two edge sites of the array are each coupled to an auxiliary damped cavity. (b) Propagating frequency band of the coupled-cavity array. (c) Schematic diagram of the long-range atom-atom interaction. The parametric drives amplify both the localization length ($\propto e^r$) of the single-photon bound-state wave function and the effective atom-photon coupling strength ($\propto e^{r/2}$), enabling the long-distance coupling between two atoms.

Moreover, each cavity of the array is subjected to a two-photon drive, described by the Hamiltonian $H_d = \eta \sum_n (a_n^{\dagger 2} e^{-i\omega_s t} e^{-i\phi} + \text{H.c.})$, where η is the two-photon driving amplitude, ω_s is its driving frequency, and ϕ is the associated phase. Experimentally, the parametric drives have been implemented with different kinds of architectures, such as flux-modulated Josephson parametric amplifiers in the microwave regime [33–37] and $\chi^{(2)}$ nonlinear crystals in the optical domain [38–40]. In addition, we assume that two edge sites of the array are each coupled to an auxiliary damped cavity, which is described by the Hamiltonian $H_A = \omega_A (A_{-N}^\dagger A_{-N} + A_N^\dagger A_N) - J_0 (A_{-N}^\dagger a_{-N} + A_N^\dagger a_N + \text{H.c.})$. As discussed below, these two auxiliary cavities constitute the main dissipative channels of this system and are used to stabilize a pure squeezed vacuum state of the internal cavities. In the rotating frame at the frequency $\omega_s/2$, the Hamiltonian of the whole system takes the form

$$H = \Delta_A (A_{-N}^\dagger A_{-N} + A_N^\dagger A_N) + \Delta_a \sum_n a_n^\dagger a_n + \Delta_q \sum_x \sigma_+^x \sigma_-^x - \left[\sum_n \left(J a_n^\dagger a_{n+1} - \eta a_n^{\dagger 2} e^{-i\phi} \right) + J_0 (A_{-N}^\dagger a_{-N} + A_N^\dagger a_N) - G (a_j^\dagger \sigma_-^A + a_l^\dagger \sigma_-^B) + \text{H.c.} \right], \tag{2}$$

where $\Delta_A = \omega_A - \omega_s/2$, $\Delta_a = \omega_a - \omega_s/2$, and $\Delta_q = \omega_q - \omega_s/2$ are the detunings. Here we assume that Δ_A, Δ_a, and Δ_q are by far the largest parameters in the system dynamics. This assumption allows us to neglect many nonresonant processes, and the resulting quasi-resonant dynamics shows highly enhanced atom-field interaction similar to the results of Refs. [41–44]. Specifically, it is convenient to perform the Bogoliubov squeezing transformation $a_n = \beta_n \cosh(r) - \beta_n^\dagger e^{-i\phi} \sinh(r)$, which diagonalizes the Hamiltonian of each parametrically driven cavity, where $r = \frac{1}{4} \ln[(\Delta_a + 2\eta)/(\Delta_a - 2\eta)]$ is the squeezing parameter. In this squeezed frame, the detuning of the modes β_n is given by $\Delta_s = \Delta_a/\cosh(2r)$. Additionally, we assume that the auxiliary cavities are resonant with these modes, corresponding to $\Delta_A = \Delta_s$. Consequently, the total Hamiltonian can be expressed as follows:

$$\begin{aligned} H_S = {} & \Delta_s (A_{-N}^\dagger A_{-N} + A_N^\dagger A_N) + \Delta_s \sum_n \beta_n^\dagger \beta_n + \Delta_q \sum_x \sigma_+^x \sigma_-^x \\ & - \Big[J \cosh(2r) \sum_n \beta_n^\dagger \beta_{n+1} + J_0 \cosh(r) (A_{-N}^\dagger \beta_{-N} + A_N^\dagger \beta_N) - G \cosh(r) (\beta_j^\dagger \sigma_-^A + \beta_l^\dagger \sigma_-^B) \\ & - J \sinh(2r) \sum_n \beta_n^\dagger \beta_{n+1}^\dagger e^{-i\phi} - J_0 \sinh(r) (A_{-N}^\dagger \beta_{-N}^\dagger + A_N^\dagger \beta_N^\dagger) e^{-i\phi} + G \sinh(r) (\beta_j^\dagger \sigma_+^A + \beta_l^\dagger \sigma_+^B) e^{-i\phi} + \text{H.c.} \Big]. \end{aligned} \tag{3}$$

In particular, H_S can be simplified by performing a rotating wave approximation that consists in dropping nonresonant fast-oscillating terms (which can be easily identified in the interaction picture) characterized by an interaction strength much smaller than the corresponding frequency. Specifically, in the limit $2\Delta_s \gg J_0 \sinh(r), J \sinh(2r)$, and $\Delta_s + \Delta_q \gg G \sinh(r)$, the Hamiltonian (3) can be approximated as

$$H_S' = \Delta_s (A_{-N}^\dagger A_{-N} + A_N^\dagger A_N) + \Delta_s \sum_n \beta_n^\dagger \beta_n + \Delta_q \sum_x \sigma_+^x \sigma_-^x - \left[\mathcal{J} \sum_n \beta_n^\dagger \beta_{n+1} + \mathcal{J}_0 (A_{-N}^\dagger \beta_{-N} + A_N^\dagger \beta_N) - \mathcal{G} (\beta_j^\dagger \sigma_-^A + \beta_l^\dagger \sigma_-^B) + \text{H.c.} \right], \tag{4}$$

where $\mathcal{J}_0 = J_0\cosh(r)$, $\mathcal{J} = J\cosh(2r)$, and $\mathcal{G} = G\cosh(r)$ are the modified coupling strengths. Remarkably, the cavity-cavity and atom-cavity couplings can be greatly enhanced due to the amplified fluctuations of the squeezed photons. This constitutes the key ingredients for realizing a long-distance atom-atom interaction.

Let us now introduce the dissipation of the auxiliary cavities, while we assume that the dissipation of the internal cavities is comparatively negligible. Such a scenario is commonly observed in these kinds of systems [25]. Then, the dynamics of the whole system is described by the quantum master equation

$$\dot{\rho}_S = -i[H_S', \rho_S] + \gamma \sum_x \mathcal{L}[\sigma_-^x]\rho_S + \kappa\mathcal{L}[A_{-N}]\rho_S + \kappa\mathcal{L}[A_N]\rho_S, \tag{5}$$

where $\mathcal{L}[O]\rho = (2O\rho O^\dagger - \rho OO^\dagger - OO^\dagger\rho)/2$ is the Lindblad operator for a given operator O, γ is the atomic spontaneous emission rate, and κ is the decay rate of the auxiliary damped cavity. Here, we consider that the auxiliary cavities A_{-N} and A_N have a large dissipation, i.e., $\kappa \gg \mathcal{J}_0$. After adiabatically eliminating the auxiliary cavities, we obtain the reduced master equation

$$\dot{\rho}_s = -i[H_s, \rho_s] + \gamma \sum_x \mathcal{L}[\sigma_-^x]\rho_s + \kappa_s\mathcal{L}[\beta_{-N}]\rho_s + \kappa_s\mathcal{L}[\beta_N]\rho_s, \tag{6}$$

where

$$H_s = \Delta_s \sum_n \beta_n^\dagger\beta_n + \Delta_q \sum_x \sigma_+^x\sigma_-^x - \left[\mathcal{J}\sum_n \beta_n^\dagger\beta_{n+1} - \mathcal{G}(\beta_j^\dagger\sigma_-^A + \beta_l^\dagger\sigma_-^B) + \text{H.c.}\right]. \tag{7}$$

Here, $\kappa_s = \mathcal{J}_0^2/\kappa$ is the effective decay rate of the squeezed modes β_{-N} and β_N. This expression entails that, in the squeezed representation, the dissipation of the auxiliary cavities drives the array to the vacuum, which is a pure squeezed state in the original frame [45]. Besides, in the dispersive regime, the dissipation has a negligible effect on the atoms for a sufficiently large array. So, the main dynamics of our system are well described by the Hamiltonian (7) with the array in the squeezed vacuum. The following analysis exploits this result.

To better understand the basic system dynamics, here we assume that the number of cavities is sufficiently large, and it is much larger than the atomic separation $2N + 1 \gg |l - j|$. In this case, the auxiliary cavities primarily serve to justify the utilization of the squeezed vacuum as the state of the array that mediates the interaction between the atoms discussed below. However, they do not play any other significant role in the dynamics of the system. So, we can simplify the model by assuming periodic boundary conditions for the array and perform the Fourier transformation $\beta_n = \sum_k \beta_k e^{-ikn}/\sqrt{2N+1}$ with $k \in [-\pi, \pi]$. Then, the Hamiltonian H_s in Eq. (7) can be transformed into the momentum space

$$H_{s,k} = \sum_k \Delta_s^k \beta_k^\dagger\beta_k + \Delta_q \sum_x \sigma_+^x\sigma_-^x + \sum_k \mathcal{G}_k(\beta_k^\dagger\sigma_-^A e^{ikj} + \beta_k^\dagger\sigma_-^B e^{ikl} + \text{H.c.}), \tag{8}$$

where $\mathcal{G}_k = \mathcal{G}/\sqrt{2N+1}$, and $\Delta_s^k = \Delta_s - 2\mathcal{J}\cos(k)$ is the dispersion relation, as seen in Fig. 1(b). We stress here that there is a sharp difference with respect to the previous works without two-photon drives for the generation of long-range interactions [18–25]. In our scheme, the presence of parametric drives makes both the propagating frequency band $4\mathcal{J}$ [see Fig. 1(c)] and the coupling strength $\mathcal{G}_k$ proportional to a hyperbolic cosine function of r, so that they both increase with r. Consequently, as discussed in detail below, on the one hand the broadened band results in an amplified localization length of the single-photon bound-state wave function. On the other, the enhanced coupling corresponds to an enhanced effective atom-photon coupling strength. These two effects result in the increased range and strength of the interaction between the two distant atoms. In the following, we employ the model of Eq. (8) to analyze the dynamics of the two atoms in the dispersive regime, which is characterized by a large detuning between the atomic transition frequency and the band-edge frequency of the array. In this regime, it is reasonable to expect that our approximated model faithfully captures the essential features of the atomic dynamics in a finite system, which can be realistically achieved in experiments [25].

III. ENHANCING THE LONG-RANGE INTERACTION BETWEEN TWO ATOMS

Let us first consider the coupling of the single atom A to the coupled-cavity array. We note that the Hamiltonian (8) conserves the total number of excitations, and as discussed above, it is reasonable to assume that in the squeezed representation the array is in its vacuum state, so we can focus on the single-excitation manifold. Specifically, there exists a bound state $|\Psi\rangle = \cos(\theta)|\text{Vac}\rangle|e_A\rangle + \sin(\theta)\sum_k c_k|1_k\rangle|g_A\rangle$ [18,22], where θ quantifies the degree of atom-photon hybridization, $|\text{Vac}\rangle$ is the vacuum state of the modes β_k, $|1_k\rangle = \beta_k^\dagger|\text{Vac}\rangle$ is a single-photon excitation state, and c_k is the amplitude of the single-photon component with momentum k. This single-photon bound state satisfies the eigenvalue equation $H_{s,k}|\Psi\rangle = \Delta_{BS}|\Psi\rangle$ with the eigenfrequency Δ_{BS}, which fulfills the relation $\delta = \Delta + \mathcal{G}^2/\sqrt{\delta^2 + 4\mathcal{J}\delta}$. Here, we have introduced the detunings $\delta = \Delta_{BS} - \Delta_U$ and $\Delta = \Delta_q - \Delta_U$ with $\Delta_U = \Delta_s + 2\mathcal{J}$ the upper band edge. In the following, we focus on the case of $\delta > 0$, i.e., $\Delta_{BS} > \Delta_U$, such that the bound state eigenfrequency lies above the propagating frequency band.

The photonic component of the single-photon bound state is localized exponentially around the atomic position. By utilizing the Fourier transformation $c_n = \sum_n c_k e^{-ikn}/\sqrt{2N+1}$, we can work out the amplitude c_n of the single-photon component at position n [see Appendix A for more detail],

$$c_n = \frac{(-1)^{|n-j|}e^{-\frac{|n-j|}{\xi}}}{\sqrt{\coth(1/\xi)}}, \tag{9}$$

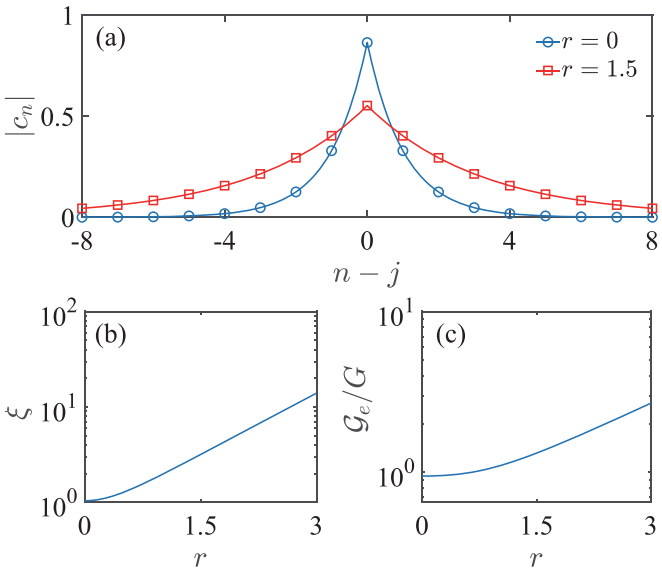

FIG. 2. (a) The photonic wave function $|c_n|$ in the real space versus the spatial position $n - j$. (b) The localization length ξ and (c) the effective atom-photon coupling strength $\mathcal{G}_e$ as a function of the squeezing parameter r. We have set $\Delta = 10G$ and $J = 10G$.

where the localization length is defined as

$$\xi = \frac{1}{\text{arccosh}(1 + \delta/2\mathcal{J})}. \tag{10}$$

We can see from Fig. 2(a) that the photonic component extends over multiple sites and exhibits an exponentially decaying envelope around the atomic position j, which is characterized by the localization length ξ. When we increase the squeezing parameter r at a fixed value of the detuning Δ between the atomic transition frequency and the upper band edge, the localization length ξ will be extended exponentially with $\xi \propto e^r$, so that the spatial distribution of the localized photon is greatly broadened [see Figs. 2(a) and 2(b)]. This is due to the enhanced cavity-cavity interaction strength $\mathcal{J}$ which, in turn, manifests itself in an enhanced propagating frequency band [see Fig. 1(b)].

In particular, the photon confined around the single atom A has the same properties as the mode of a real cavity [21]. Therefore, the coupling of a single atom to the coupled-cavity array can be well understood by mapping to the Jaynes-Cummings model with the effective atom-photon coupling strength

$$\mathcal{G}_e = \frac{\sqrt{2}\mathcal{G}}{(1 + 4\mathcal{J}/\delta)^{\frac{1}{4}}} \tag{11}$$

and the effective atom-photon detuning $\Delta_e = \Delta_q - \sum_k \Delta_k |c_k|^2 = \Delta + \delta/(1 + \delta/2\mathcal{J})$. In Fig. 2(c), we plot the effective atom-photon coupling strength $\mathcal{G}_e$ as a function of the squeezing parameter r. As the squeezing parameter r increases, the effective atom-photon coupling strength will exhibit an exponential enhancement with $\mathcal{G}_e \propto e^{r/2}$.

Let us now consider two spatially separated atoms interacting with the coupled-cavity array. In the dispersive regime $\Delta_e \gg \mathcal{G}_e$ ($\delta \approx \Delta$), the effective cavity will mediate a coherent atom-atom interaction via the exchange of virtual photons

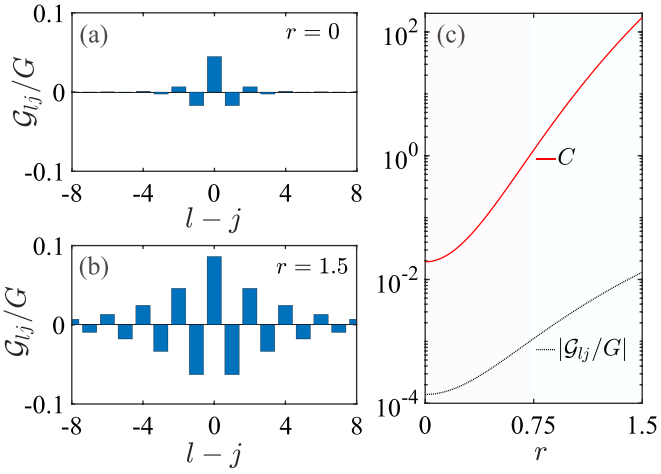

FIG. 3. (a) and (b) The photon-mediated atom-atom coupling strength $\mathcal{G}_{lj}$ as a function of the atomic separation $l - j$. (c) The absolute value of the coupling strength $|\mathcal{G}_{lj}|$ and the cooperativity C versus the squeezing parameter r for the case of two distant atoms $|l - j| = 6$, where we set $\gamma = 0.001G$. The other parameters are the same as in Fig. 2.

[18]. By tracing out the modes β_k in Hamiltonian (4), we can obtain the effective Hamiltonian in the interaction picture as [see Appendix B for more detail]

$$H_{AB} = \mathcal{G}_{lj}(\sigma_+^A \sigma_-^B + \sigma_-^A \sigma_+^B) \tag{12}$$

with

$$\mathcal{G}_{lj} = (-1)^{|l-j|} \frac{\mathcal{G}_e'^2}{2\Delta} e^{-\frac{|l-j|}{\xi'}}, \tag{13}$$

where we have the effective atom-photon coupling strength $\mathcal{G}_e' = \sqrt{2}\mathcal{G}/(1 + 4\mathcal{J}/\Delta)^{\frac{1}{4}} \approx \mathcal{G}_e$, and the localization length $\xi' = 1/\text{arccosh}(1 + \Delta/2\mathcal{J}) \approx \xi$. Note that the photon-mediated interaction between two atoms naturally inherits the property of the single-photon bound state. Thus, the resulting atom-atom interaction is exponentially localized in the real space with $\mathcal{G}_{lj} \propto e^{-\frac{|l-j|}{\xi'}}$, which is consistent with previous studies [18–25]. However, the unique feature here is that both ξ' and $\mathcal{G}_e'$ increase with the squeezing parameter r, and this will induce a significant enhancement of the photon-mediated atom-atom coupling strength $\mathcal{G}_{lj}$. To demonstrate this, we plot the coupling strength $\mathcal{G}_{lj}$ as a function of the interatomic distance $l - j$ without and with the parametric driving process in Figs. 3(a) and 3(b). For the case of $r = 0$, the photon-mediated atom-atom coupling decays rapidly as the atomic separation increases, which results in a short-distance atom-atom interaction [see Fig. 3(a)]. This is in stark contrast to $r \neq 0$, where the two-photon parametric interactions significantly suppress the exponential decay behavior of the photon-mediated atom-atom interaction [see Fig. 3(b)]. Hence, even if the two atoms are separated by a relatively large distance, they can still be strongly coupled to each other.

To quantify the enhancement of $\mathcal{G}_{lj}$, we further introduce the cooperativity $C = \mathcal{G}_{lj}^2/\gamma^2$ with the atomic spontaneous emission rate γ. In Fig. 3(c), we plot the photon-mediated atom-atom coupling strength $|\mathcal{G}_{lj}|$ and the cooperativity C as a function of the squeezing parameter r for two distant atoms $|l - j| = 6$. Without the two-photon driving process ($r = 0$),

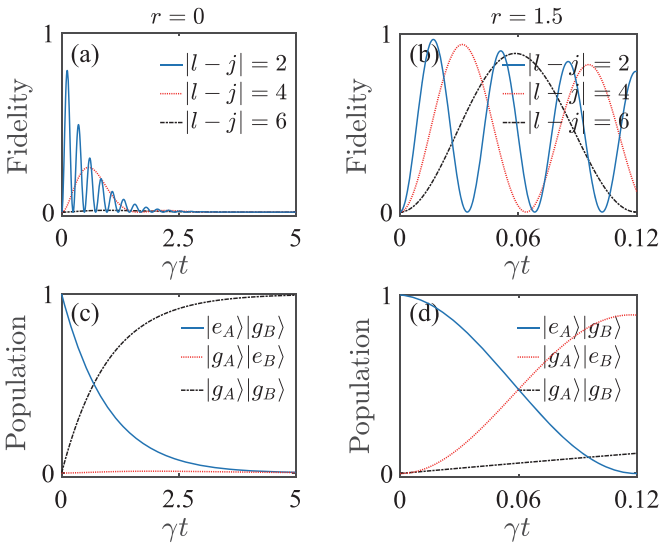

FIG. 4. Numerical simulations of (a) and (b) the fidelity F and (c) and (d) the populations of two separated atoms versus the time t. The results given in (c) and (d) are for $|l-j|=6$ and the other parameters are the same as in Fig. 3.

we obtain the relatively small values $|\mathcal{G}_{lj}| \approx 1.38\times10^{-4}G$ and $C \approx 0.02$, such that the distant atoms are very weakly coupled. However, these values are strongly enhanced when r is increased, and for $r > 0.723$, we have $|\mathcal{G}_{lj}| > 1\times10^{-3}G$ and $C > 1$, i.e., the atom-atom interaction enters into the strong-coupling regime.

IV. LONG-RANGE ENTANGLEMENT AND QUANTUM INFORMATION TRANSFER OF TWO ATOMS

As an application, we now discuss how to achieve long-distance entanglement and quantum information transfer between two separated atoms. If the two atoms initially are prepared in the state $|\phi(0)\rangle = |e_A\rangle|g_B\rangle$ and the atomic decay is negligible, one can generate a maximally entangled state $|S\rangle = (|e_A\rangle|g_B\rangle - i(-1)^{|l-j|}|g_A\rangle|e_B\rangle)/\sqrt{2}$ at the time $t = \pi/(4|\mathcal{G}_{lj}|)$. Similarly, the state of the atom A in the initial state $|\phi(0)\rangle = (\alpha_1|g_A\rangle + \alpha_2|e_A\rangle)|g_B\rangle$ will be transferred to the atom B with $|\phi(t)\rangle = |g_A\rangle(\alpha_1|g_B\rangle - i(-1)^{|l-j|}\alpha_2|e_B\rangle)$ at the time $t = \pi/(2|\mathcal{G}_{lj}|)$.

In the presence of the atomic decoherence, we can use the quantum master equation $\dot{\rho}_r = -i[H_{AB}, \rho_r] + \gamma\sum_x \mathcal{L}[\sigma_-^x]\rho_r$ to characterize the dynamics of entanglement and populations of the two separated atoms. The entanglement of two atoms may be quantified by the fidelity $F = \mathrm{Tr}(\rho_r|S\rangle\langle S|)$ [46]. Figure 4 illustrates the numerical results of the time evolution of the fidelity and atomic populations, highlighting the effects of the enhanced cooperativity demonstrated in Fig. 3(c). Specifically, for the chosen parameters, when the atomic distance is large and $r = 0$, entanglement generation [see Fig. 4(a)] and population transfer [see Fig. 4(c)] are unfeasible. However, both tasks are made efficient by the two-photon drives, as shown in Figs. 4(b) and 4(d).

V. DISCUSSION AND CONCLUSIONS

Finally, we discuss the experimental implementations of our scheme. A promising platform is based on superconducting circuits with their advanced controllability and versatile interfaces [47]. Specifically, the cavity array can be made of superconducting microwave cavities embedded with superconducting quantum interference device (SQUID) loops, and the two-photon drives can be implemented by modulating the flux threading the SQUID loops [33–37]. We note that the strength of the two-photon drives should be quite large, of the order of $\Delta_a/2$. In this devices, the value of η is proportional to the strength of the flux modulation and the ultimate limit of the two-photon strength is set by the instability of the parametric process. When the flux modulation at frequency ω_s is in resonance with twice the frequency of the microwave mode $\omega_s = 2\omega_a$, the strength of the two-photon drive cannot exceed the relaxation rate of the microwave mode, otherwise the system becomes unstable. The relaxation rate can be quite small, so that under these conditions it is clearly not possible to achieve the values of η needed for our proposal. However, our system works in a different regime. We assume that the parametric process is not resonant, but it is detuned by the value Δ_a, i.e., $\omega_s = 2(\omega_a - \Delta_a)$. In this situation the instability is moved to much larger values and the system is stable for any value of η^2 that does not exceed $\Delta_a^2/4$ by more than the square of the relaxation rate. This is the case in our proposal. For this reason, it should be possible, in principle, to use sufficiently strong flux modulation and achieve the large values of η used in this work (see Ref. [48] for a recent theoretical proposal which employs detuned parametric drives). This would allow us to achieve long-range interactions between superconducting qubits [20,23–27] or Rydberg atoms [49,50] coupled to microwave cavities. Alternatively, in the optical regime, two atomic emitters could be coupled to an array of optical cavities [28–32]. In this case, the parametric drives can be realized by degenerate parametric downconversion [38–40].

In summary, we have proposed an efficient scheme for enhancing long-range interaction between two atoms mediated by a coupled-cavity array. We show that when each site of the photonic chain is subjected to a parametric drive, the localization length of the single-photon bound-state wave function and the effective atom-photon coupling strength are significantly increased, enabling a huge enhancement of the coherent photon-mediated interaction between two distant atoms. So, long-range entanglement and quantum information transfer between two remote atoms can be achieved. Our proposal is general, and can also be applied to other quantum systems, such as phononic [51,52] and magnonic crystals [53,54].

ACKNOWLEDGMENTS

We acknowledge financial support from the National Natural Science Foundation of China (Grants No. 11704306 and No. 12074307) and financial support from NQSTI within PNRR MUR Project No. PE0000023-NQSTI.

APPENDIX A: LOCALIZATION LENGTH OF SINGLE-PHOTON BOUND-STATE WAVE FUNCTION

In this section, we describe the procedure to derive the single-photon bound-state wave function and corresponding localization length. If we consider the atom A interacting with the coupled-cavity array, the single-photon bound state can be written as

$$|\Psi\rangle = \cos(\theta)|\text{Vac}\rangle|e_A\rangle + \sin(\theta)\sum_k c_k|1_k\rangle|g_A\rangle. \tag{A1}$$

By substituting $|\Psi\rangle$ into the Schrödinger equation with $H_{s,k}|\Psi\rangle = \Delta_{BS}|\Psi\rangle$, where $H_{s,k}$ is defined in Eq. (8) of the main text, one can obtain the coupled equations

$$\begin{aligned}\cos(\theta)(\Delta_{BS}-\Delta_q) &= \frac{\mathcal{G}}{\sqrt{2N+1}}\sum_k \sin(\theta)c_k e^{-ikj},\\ \sin(\theta)\big(\Delta_{BS}-\Delta_s^k\big)c_k &= \frac{\mathcal{G}}{\sqrt{2N+1}}\cos(\theta)e^{ikj}.\end{aligned} \tag{A2}$$

Solving these equations will yield

$$\begin{aligned}c_k &= \frac{\mathcal{G}e^{ikj}}{\tan(\theta)\sqrt{2N+1}[(\delta+2\mathcal{J})+2\mathcal{J}\cos(k)]},\\ \delta &= \Delta + \int_{-\pi}^{\pi}\frac{\mathcal{G}^2}{(\delta+2\mathcal{J})+2\mathcal{J}\cos(k)}\frac{dk}{2\pi},\\ \tan^2(\theta) &= \int_{-\pi}^{\pi}\frac{\mathcal{G}^2}{[(\delta+2\mathcal{J})+2\mathcal{J}\cos(k)]^2}\frac{dk}{2\pi}\end{aligned} \tag{A3}$$

with $\delta = \Delta_{BS} - \Delta_U$ and $\Delta = \Delta_q - \Delta_U$. In Eq. (A3), we substituted the sums with integrals according to $\sum_k[1/(2N+1)] \to \int_{-\pi}^{\pi}(dk/2\pi)$. Integrating Eq. (A3) for $\delta > 0$ gives us

$$\begin{aligned}\tan(\theta) &= \mathcal{G}\sqrt{\frac{\delta+2\mathcal{J}}{(\delta^2+4\mathcal{J}\delta)^{\frac{3}{2}}}},\\ \delta &= \Delta + \frac{\mathcal{G}^2}{\sqrt{\delta^2+4\mathcal{J}\delta}}\\ &= \Delta + \frac{\mathcal{G}_e^2}{2\delta},\end{aligned} \tag{A4}$$

where $\mathcal{G}_e = \sqrt{2}\mathcal{G}/(1+4\mathcal{J}/\delta)^{\frac{1}{4}}$ is the effective atom-photon coupling strength. Substituting Eq. (A4) into Eq. (A3) and using the Fourier transformation $c_n = \sum_k c_k e^{-ikn}/\sqrt{2N+1}$, we can obtain the single-photon bound-state wave function in the real space

$$\begin{aligned}c_n &= \int_{-\pi}^{\pi}\frac{\mathcal{G}e^{-ik(n-j)}}{\tan(\theta)[(\delta+2\mathcal{J})+2\mathcal{J}\cos(k)]}\frac{dk}{2\pi}\\ &= \frac{(-1)^{|n-j|}e^{-\frac{|n-j|}{\xi}}}{\sqrt{\coth(1/\xi)}}\end{aligned} \tag{A5}$$

with

$$\xi = \frac{1}{\text{arccosh}(1+\delta/2\mathcal{J})}. \tag{A6}$$

Obviously, the photonic component has an exponentially decaying envelope around the atomic position j, and ξ denotes the localization length.

APPENDIX B: PHOTON-MEDIATED ATOM-ATOM INTERACTION

In this section, we show how to derive the photon-mediated interaction of atoms. In the interaction picture, we can obtain the coherent interaction between the atoms and the photonic modes

$$\begin{aligned}H_{s,k}^I = \sum_k \frac{\mathcal{G}}{\sqrt{2N+1}}[&(\beta_k^\dagger\sigma_-^A e^{ikj} + \beta_k^\dagger\sigma_-^B e^{ikl})e^{-i(\Delta_q-\Delta_s^k)}\\ &+ (\beta_k\sigma_+^A e^{-ikj} + \beta_k\sigma_+^B e^{-ikl})e^{i(\Delta_q-\Delta_s^k)}].\end{aligned} \tag{B1}$$

In the dispersive regime, the bound state gives rise to an effective dipole-dipole interaction between the two atoms. By eliminating the photonic modes, the atom-atom interaction is described by the effective Hamiltonian

$$H_{AB} = \mathcal{G}_{lj}(\sigma_+^A\sigma_-^B + \sigma_-^A\sigma_+^B), \tag{B2}$$

where the photon-mediated atom-atom coupling strength is given by

$$\begin{aligned}\mathcal{G}_{lj} &= \int_{-\pi}^{\pi}\frac{\mathcal{G}^2e^{ik(l-j)}}{(\Delta+2\mathcal{J})+2\mathcal{J}\cos(k)}\frac{dk}{2\pi}\\ &= (-1)^{|l-j|}\frac{\mathcal{G}^2}{\sqrt{\Delta^2+4\Delta J}}e^{-\frac{|l-j|}{\xi'}},\\ &= (-1)^{|l-j|}\frac{[\sqrt{2}\mathcal{G}/(1+4\mathcal{J}/\Delta)^{\frac{1}{4}}]^2}{2\Delta}e^{-\frac{|l-j|}{\xi'}}.\end{aligned} \tag{B3}$$

Here $\xi' = \frac{1}{\text{arccosh}(1+\Delta/2\mathcal{J})}$ is the localization length, which characterizes the interaction range between two spatially separated atoms. These equations are consistent with the results of the previous section in the dispersive regime where $\delta \sim \Delta$.

[1] D. J. van Woerkom, P. Scarlino, J. H. Ungerer, C. Müller, J. V. Koski, A. J. Landig, C. Reichl, W. Wegscheider, T. Ihn, K. Ensslin, and A. Wallraff, Phys. Rev. X **8**, 041018 (2018).

[2] V. D. Vaidya, Y. Guo, R. M. Kroeze, K. E. Ballantine, A. J. Kollár, J. Keeling, and B. L. Lev, Phys. Rev. X **8**, 011002 (2018).

[3] R. E. Evans, M. K. Bhaskar, D. D. Sukachev, C. T. Nguyen, A. Sipahigil, M. J. Burek, B. Machielse, G. H. Zhang, A. S. Zibrov, E. Bielejec, H. Park, M. Lončar, and M. D. Lukin, Science **362**, 662 (2018).

[4] F. Borjans, X. G. Croot, X. Mi, M. J. Gullans, and J. R. Petta, Nature (London) **577**, 195 (2020).

[5] A. W. Glaetzle, R. M. W. van Bijnen, P. Zoller, and W. Lechner, Nat. Commun. **8**, 15813 (2017).

[6] C. L. Degen, F. Reinhard, and P. Cappellaro, Rev. Mod. Phys. **89**, 035002 (2017).

[7] C. Schimpf, M. Reindl, D. Huber, B. Lehner, S. F. C. D. Silva, S. Manna, M. Vyvlecka, P. Walther, and A. Rastelli, Sci. Adv. **7**, eabe8905 (2021).

[8] F. Arute, K. Arya, R. Babbush, D. Bacon, J. C. Bardin, R. Barends, R. Biswas, S. Boixo, F. G. S. L. Brandao, D. A. Buell *et al.*, Nature (London) **574**, 505 (2019).

[9] M. Gong, S. Wang, C. Zha, M.-C. Chen, H.-L. Huang, Y. Wu, Q. Zhu, Y. Zhao, S. Li, S. Guo *et al.*, Science **372**, 948 (2021).

[10] A. J. Sigillito, M. J. Gullans, L. F. Edge, M. Borselli, and J. R. Petta, npj Quantum Inf. **5**, 110 (2019).

[11] F. Marxer, A. Vepsalainen, S. W. Jolin, J. Tuorila, A. Landra, C. Ockeloen-Korppi, W. Liu, O. Ahonen, A. Auer, L. Belzane *et al.*, PRX Quantum **4**, 010314 (2023).

[12] W. Pfaff, B. J. Hensen, H. Bernien, S. B. van Dam, M. S. Blok, T. H. Taminiau, M. J. Tiggelman, R. N. Schouten, M. Markham, D. J. Twitchen, and R. Hanson, Science **345**, 532 (2014).

[13] W. D. Newman, C. L. Cortes, A. Afshar, K. Cadien, A. Meldrum, R. Fedosejevs, and Z. Jacob, Sci. Adv. **4**, eaar5278 (2018).

[14] B. Žunkovič, M. Heyl, M. Knap, and A. Silva, Phys. Rev. Lett. **120**, 130601 (2018).

[15] A. Campa, T. Dauxois, and S. Ruffo, Phys. Rep. **480**, 57 (2009).

[16] M. F. Maghrebi, Z.-X. Gong, and A. V. Gorshkov, Phys. Rev. Lett. **119**, 023001 (2017).

[17] P. Richerme, Z.-X. Gong, A. Lee, C. Senko, J. Smith, M. Foss-Feig, S. Michalakis, A. V. Gorshkov, and C. Monroe, Nature (London) **511**, 198 (2014).

[18] J. S. Douglas, H. Habibian, C.-L. Hung, A. V. Gorshkov, H. J. Kimble, and D. E. Chang, Nat. Photon. **9**, 326 (2015).

[19] A. González-Tudela, C.-L. Hung, D. E. Chang, J. I. Cirac, and H. J. Kimble, Nat. Photon. **9**, 320 (2015).

[20] Y. Liu and A. A. Houck, Nat. Phys. **13**, 48 (2017).

[21] D. E. Chang, J. S. Douglas, A. González-Tudela, C.-L. Hung, and H. J. Kimble, Rev. Mod. Phys. **90**, 031002 (2018).

[22] M. Bello, G. Platero, J. I. Cirac, and A. González-Tudela, Sci. Adv. **5**, eaaw0297 (2019).

[23] N. M. Sundaresan, R. Lundgren, G. Zhu, A. V. Gorshkov, and A. A. Houck, Phys. Rev. X **9**, 011021 (2019).

[24] E. Kim, X. Zhang, V. S. Ferreira, J. Banker, J. K. Iverson, A. Sipahigil, M. Bello, A. González-Tudela, M. Mirhosseini, and O. Painter, Phys. Rev. X **11**, 011015 (2021).

[25] M. Scigliuzzo, G. Calajò, F. Ciccarello, D. Perez Lozano, A. Bengtsson, P. Scarlino, A. Wallraff, D. Chang, P. Delsing, and S. Gasparinetti, Phys. Rev. X **12**, 031036 (2022).

[26] V. S. Ferreira, J. Banker, A. Sipahigil, M. H. Matheny, A. J. Keller, E. Kim, M. Mirhosseini, and O. Painter, Phys. Rev. X **11**, 041043 (2021).

[27] X. Zhang, E. Kim, D. K. Mark, S. Choi, and O. Painter, Science **379**, 278 (2023).

[28] J. D. Thompson, T. G. Tiecke, N. P. de Leon, J. Feist, A. V. Akimov, M. Gullans, A. S. Zibrov, V. Vuletić, and M. D. Lukin, Science **340**, 1202 (2013).

[29] T. G. Tiecke, J. D. Thompson, N. P. de Leon, L. R. Liu, V. Vuletić, and M. D. Lukin, Nature (London) **508**, 241 (2014).

[30] A. Reiserer and G. Rempe, Rev. Mod. Phys. **87**, 1379 (2015).

[31] S.-P. Yu, J. A. Muniz, C.-L. Hung, and H. J. Kimble, Proc. Natl. Acad. Sci. **116**, 12743 (2019).

[32] E. Will, L. Masters, A. Rauschenbeutel, M. Scheucher, and J. Volz, Phys. Rev. Lett. **126**, 233602 (2021).

[33] I. Siddiqi, R. Vijay, F. Pierre, C. M. Wilson, M. Metcalfe, C. Rigetti, L. Frunzio, and M. H. Devoret, Phys. Rev. Lett. **93**, 207002 (2004).

[34] T. Yamamoto, K. Inomata, M. Watanabe, K. Matsuba, T. Miyazaki, W. D. Oliver, Y. Nakamura, and J. S. Tsai, Appl. Phys. Lett. **93**, 042510 (2008).

[35] X. Zhou, V. Schmitt, P. Bertet, D. Vion, W. Wustmann, V. Shumeiko, and D. Esteve, Phys. Rev. B **89**, 214517 (2014).

[36] M. Malnou, D. A. Palken, B. M. Brubaker, L. R. Vale, G. C. Hilton, and K. W. Lehnert, Phys. Rev. X **9**, 021023 (2019).

[37] K. M. Backes, D. A. Palken, S. Al Kenany, B. M. Brubaker, S. B. Cahn, A. Droster, G. C. Hilton, S. Ghosh, H. Jackson, S. K. Lamoreaux*et al.*, Nature (London) **590**, 238 (2021).

[38] J. U. Fürst, D. V. Strekalov, D. Elser, M. Lassen, U. L. Andersen, C. Marquardt, and G. Leuchs, Phys. Rev. Lett. **104**, 153901 (2010).

[39] R. Gao, H. Zhang, F. Bo, W. Fang, Z. Hao, N. Yao, J. Lin, J. Guan, L. Deng, M. Wang, L. Qiao, and Y. Cheng, New J. Phys. **23**, 123027 (2021).

[40] F. Meylahn, B. Willke, and H. Vahlbruch, Phys. Rev. Lett. **129**, 121103 (2022).

[41] X.-Y. Lü, Y. Wu, J. R. Johansson, H. Jing, J. Zhang, and F. Nori, Phys. Rev. Lett. **114**, 093602 (2015).

[42] M.-A. Lemonde, N. Didier, and A. A. Clerk, Nat. Commun. **7**, 11338 (2016).

[43] W. Qin, A. Miranowicz, P.-B. Li, X.-Y. Lü, J. Q. You, and F. Nori, Phys. Rev. Lett. **120**, 093601 (2018).

[44] C. Leroux, L. C. G. Govia, and A. A. Clerk, Phys. Rev. Lett. **120**, 093602 (2018).

[45] J.-k. Xie, S.-l. Ma, Y.-l. Ren, X.-k. Li, and F.-l. Li, Phys. Rev. A **101**, 012348 (2020).

[46] M. A. Nielsen and I. L. Chuang, *Quantum Computation and Quantum Information: 10th Anniversary Edition* (Cambridge University Press, Cambridge, 2010).

[47] A. Blais, A. L. Grimsmo, S. M. Girvin, and A. Wallraff, Rev. Mod. Phys. **93**, 025005 (2021).

[48] A. Metelmann, O. Lanes, T.-Z. Chien, A. McDonald, M. Hatridge, and A. A. Clerk, arXiv:2208.00024.

[49] A. A. Morgan and S. D. Hogan, Phys. Rev. Lett. **124**, 193604 (2020).

[50] A. Kumar, A. Suleymanzade, M. Stone, L. Taneja, A. Anferov, D. I. Schuster, and J. Simon, Nature (London) **615**, 614 (2023).

[51] Y. Wang, B. Yousefzadeh, H. Chen, H. Nassar, G. Huang, and C. Daraio, Phys. Rev. Lett. **121**, 194301 (2018).

[52] S. C. Burd, R. Srinivas, H. M. Knaack, W. Ge, A. C. Wilson, D. J. Wineland, D. Leibfried, J. J. Bollinger, D. T. C. Allcock, and D. H. Slichter, Nat. Phys. **17**, 898 (2021).

[53] P. Andrich, C. F. de las Casas, X. Liu, H. L. Bretscher, J. R. Berman, F. J. Heremans, P. F. Nealey, and D. D. Awschalom, npj Quantum Inf. **3**, 28 (2017).

[54] F. Kranzl, S. Birnkammer, M. K. Joshi, A. Bastianello, R. Blatt, M. Knap, and C. F. Roos, Phys. Rev. X **13**, 031017 (2023).